Knowledge-based and data-driven causal analysis for Galerkin models exemplified by turbulent shear flows

Yongyi Wang[1,2,3], **Jiaqing Kou**[1,2,3] **and Weiwei Zhang**[1,2,3]

1 School of Aeronautics, Northwestern Polytechnical University, Xi'an 710072, China
2 International Joint Institute of Artificial Intelligence on Fluid Mechanics, Northwestern Polytechnical University, Xi'an, 710072, China
3 National Key Laboratory of Aircraft Configuration Design, Xi'an 710072, China

E-mail: jqkou@nwpu.edu.cn

Abstract. In this work, we propose a causal analysis framework for low-dimensional Galerkin models by coupling knowledge-based and data-driven methods, which is verified on a 9-equation shear flow model by Moehlis et al. [39] The knowledge-based method performs a qualitative analysis of causality between Galerkin modes using mathematical and physical information. Two types of mode interaction are identified by the knowledge, namely transfer pair between two modes and triad interaction between three modes. The data-driven analysis utilizes a modified Granger causality test that incorporates nonlinear terms and employs windowed sampling of time-dependent mode coefficients. It is shown that the identified causality from knowledge is also characterized by the data-driven analysis. The modified Granger causality exhibits robust performance and compensates for the inability of knowledge-based approach to analyse quantitatively. To demonstrate the practical applications of causal analysis, causality is utilized to guide the design of flow control, the extreme events in turbulent shear flow are successfully suppressed by applying intermittent body forces. The present work offers a promising tool for causal inference and control of complex flows.

Keywords: Causal inference, reduced-order models, flow control

1. Introduction

Despite the employment of diverse research instruments and methodologies, causality has consistently been the focus of fluid mechanics and other scientific domains [1,2]. Confronted with intricate challenges in fluid mechanics, such as turbulence, fluid-structure interaction (FSI), and multiphase flow, our current understanding remains limited. Experiments and simulations are capable of reproducing various complex flow phenomena; however, physical laws are obscured within these intricate flow phenomena. Conventional correlation analyses are used to identify statistical associations. However, these associations are often superficial and insufficient for explaining the physical laws within complex systems. By contrast, causality focuses on identifying the influences of physical phenomena, understanding the mechanisms through which these influences arise. The exploration of cause and effect in complex systems facilitates the discovery of new physical laws and the development of a deeper

understanding. Furthermore, being aware of the potential outcomes of changing conditions is instructive for engineering applications.

In recent years, an increasing number of researchers have begun to focus on data-driven causal analysis. In contrast to causal analysis based on Randomized controlled trial (RCT), which is frequently used in scientific research, data-driven causal analysis utilizes specific algorithms to directly infer causal relationships from data. The identification of causality is typically facilitated by the analysis of the transfer of information within data. To illustrate this process, consider a scenario in which variable A is the cause of variable B. It can be posited that specific information must initially appear in variable A and subsequently be conveyed to variable B. Various algorithms have been developed to quantify the transfer of information between variables, such as Granger causality [3], Effective information [4] and Transfer entropy [5]. Certain machine learning methods may also uncover causality within vast datasets [6].

Data-driven causal analysis has the potential to offer valuable solutions to a range of challenging problems in the field of fluid dynamics. Consider the complex issue of wall turbulence. Tissot et al. [7] utilized Granger causality to examine the causal relationships between the various velocity components in logarithmic layer of wall turbulence. Their findings indicated that streak breakdowns initiate jets that are perpendicular to the wall surface. Lozano-Durán et al. [8] applied transfer entropy to analyze the causal interactions between energy-containing eddies, revealing similar causal patterns between the buffer layer and the logarithmic layer. Martínez-Sánchez et al. [9] examined the causal relationships within primary POD modes in the turbulent flow surrounding a three-dimensional square cylinder, thereby laying a theoretical groundwork for investigating air pollutant dispersion in urban environments. Cremades et al. [6] used U-net to model the evolution of wall turbulence, then Shapley Additive exPlanations (SHAP) was utilized to discover region of importance in the turbulence. Lozano-Durán et al. [10] studied the impact of modifying linear terms by introducing perturbations into self-sustaining wall turbulence, revealing the mechanism of linear energy transfer from the mean flow to the fluctuating velocities. These findings may provide useful information for mechanistic studies and flow control [11]. In the study of isotropic turbulence, Jiménez successfully identified regions of importance by applying perturbations to a specific area and assessing the resulting effects. This method was applied to both two-dimensional isotropic turbulence [12] and three-dimensional isotropic turbulence [13]. Causal analysis also holds application value in fluid-structure interactions (FSI). Zhang et al. [14] revealed the causal relationship between tandem wings in uniform airflow using transfer entropy. Bagchi et al. [15] analyzed the relationship between structural oscillation and the Reynolds number in jet-induced vibrations of a cantilever beam using Pearson correlation and Granger causality. Causal analysis has also been used to investigate the relationship between variations in pressure at distinct locations within a jet [16], with the aim of identifying the regions from which aerodynamic noise originates.

However, data-driven causal analysis is not without its limitations. As a purely data-driven approach, it may yield computationally plausible yet factually false results [17,18]. Without sufficient prior knowledge for reference, it is impossible to determine the accuracy of the results, which leads to issues of interpretability and robustness in causal inference. This problem is of particular concern in the field of physical research, as physical conclusions must be drawn with rigor. Thus, in this study, we have developed a hybrid approach that combines knowledge-based and data-driven causal analysis for the Galerkin model. This approach compensates for the inherent unreliability of data-driven methods by integrating prior knowledge. It enhances data-driven causal analysis techniques through the use of prior knowledge and validates the rationality of the analysis outcomes with the same knowledge base.

This paper is organized as follows. Chapter 2 and Chapter 3 elaborate on the theoretical foundations of the Galerkin model and classical Granger causality, respectively. In Chapter 4, a modified Granger causality tailored for the Galerkin model is proposed, and a newly defined segmented sampling strategy and causality identification metric is introduced. In Chapter 5, we apply knowledge-based and data-driven causal analysis to the nine-equation turbulent shear flow model proposed by Moehlis et al. [19] The two methods identify causality from qualitative and quantitative perspectives, respectively, and are able to validate each other. In order to demonstrate the potential applications of causal analysis, a causality-guided flow control method that suppresses extreme events in turbulence is proposed. Finally, the conclusions are presented in Chapter 6.

2. Galerkin model

Reduced-order models (ROMs) represent complex flow systems with low-dimensional manifolds, thereby simplifying analysis and computation, and facilitating the application of dynamical system theories and flow control [20]. The Galerkin Method (GM) is one of the commonly used approaches to construct ROMs. It projects the governing equations onto modes to obtain a set of ordinary differential equations (ODEs) that describe the temporal evolution of modal coefficients. In considering unsteady incompressible flows, the governing equations are the incompressible Navier-Stokes equations

$$\nabla \cdot \boldsymbol{u} = 0, \tag{2.1}$$

$$\frac{\partial \boldsymbol{u}}{\partial t} + (\boldsymbol{u} \cdot \nabla)\boldsymbol{u} = -\frac{1}{\rho}\nabla p + \upsilon \nabla^2 \boldsymbol{u} + \boldsymbol{f}. \tag{2.2}$$

The velocity $\boldsymbol{u}$ is divided into two components: a constant mean flow velocity $\boldsymbol{u}_0$ and a fluctuating velocity $\boldsymbol{u}'$ that varies over time. After modal projection, the high-dimensional fluctuating velocity is decomposed into a linear combination of several modes. These velocity modes are mutually orthogonal, which means that the inner product of any two modes is zero, i.e. $(\boldsymbol{\Phi_i}, \boldsymbol{\Phi_j})_\Omega = 0 \ (i \neq j)$,

$$\boldsymbol{u}(t) = \boldsymbol{u}_0 + \boldsymbol{u}'(t) = \boldsymbol{u}_0 + \sum_{i=1}^{n} a_i(t)\boldsymbol{\Phi}_i. \tag{2.3}$$

The decomposed velocity is then substituted into the incompressible Navier-Stokes equations. Following mathematical simplification [21], the final Reduced Order Model is obtained, which is a set of nonlinear ordinary differential equations for modal coefficients

$$\frac{da_i}{dt} = C_i + \sum_{j=1}^{n} D_{ij} a_j + \sum_{j=1}^{n}\sum_{k=1}^{n} Q_{ijk} a_j a_k. \tag{2.4}$$

The constant term in the equation arises from the pressure gradient, external body force, and mean flow velocity. In incompressible flows, the divergence of velocity is zero, which means the inner product of the pressure gradient and the velocity mode (the first term in the subsequent equation) is entirely dependent on the boundary conditions [22],

$$C_i = -\left(\boldsymbol{\Phi}_i, \nabla p\right)_\Omega + \left(\boldsymbol{\Phi}_i, \boldsymbol{f}\right)_\Omega - \left(\boldsymbol{\Phi}_i, \left(\boldsymbol{u}_0 \cdot \nabla\right)\boldsymbol{u}_0\right)_\Omega + \nu\left(\boldsymbol{\Phi}_i, \Delta \boldsymbol{u}_0\right)_\Omega. \tag{2.5}$$

The linear term arises from viscous dissipation and the interaction between the mean flow velocity and the fluctuating velocity under convection,

$$D_{ij} = \nu\left(\boldsymbol{\Phi}_i, \Delta \boldsymbol{u}_j\right)_\Omega - \left(\boldsymbol{\Phi}_i, (\boldsymbol{u}_0 \cdot \nabla)\boldsymbol{\Phi}_j\right)_\Omega - \left(\boldsymbol{\Phi}_i, \left(\boldsymbol{\Phi}_j \cdot \nabla\right)\boldsymbol{u}_0\right)_\Omega. \tag{2.6}$$

All quadratic terms originate from convection effects,

$$Q_{ijk} = -\left(\boldsymbol{\Phi_i}, \left(\boldsymbol{\Phi_j} \cdot \nabla\right)\boldsymbol{\Phi_k}\right)_\Omega. \tag{2.7}$$

3. Granger causality

In 1969, the renowned economist Clive Granger, motivated by Wiener's theory of prediction [23], put forward the concept of Granger causality (GC) [3]. Since its introduction, the method has been widely applied in numerous fields involving data analysis [24-27]. The fundamental concept of Granger causality is straightforward: if A is found to contribute to the prediction of future B, then A is considered a cause of B. Initially, Granger causality was applicable only to analyzing causal relationship between two variables. In 1984, Geweke introduced Conditional Granger causality (cGC) [28], expanding its application to the analysis of multivariate systems. Following the input of the data series, the Granger causality test constructs two Vector Autoregression (VAR) models to determine if the inclusion of variable A enhances the prediction of variable B. Specifically, consider a multivariate dynamical system that can be described by a VAR model

$$\boldsymbol{X} = \sum_{r=1}^{p} \boldsymbol{A}^{(r)} \boldsymbol{X}^{(r)} + \boldsymbol{\varepsilon} \tag{3.1}$$

the system comprises n variables, where $\boldsymbol{X}=\left[\boldsymbol{x}_1^t,\boldsymbol{x}_2^t,\boldsymbol{x}_3^t\cdots\boldsymbol{x}_n^t\right]^T$ is a matrix created by arranging all variable vectors in rows. $\boldsymbol{X}^{(r)}$ represents the matrix of variable vectors delayed by r orders, namely $[\boldsymbol{x}_1^{t-1},\boldsymbol{x}_2^{t-r},\boldsymbol{x}_3^{t-r}\cdots\boldsymbol{x}_n^{t-r}]^T$, and $\boldsymbol{A}^{(r)}$ is the linear dynamics matrix corresponding to $\boldsymbol{X}^{(r)}$. $\mathcal{E}$ represents the model error, which is a vector comprised of the prediction errors for n variables. To evaluate the causal effect of $\boldsymbol{x}_i$ on $\boldsymbol{x}_j$ denoted as $\mathrm{F}_{i\to j}$, a full model that includes $\boldsymbol{x}_i$ and a reduced model that excludes $\boldsymbol{x}_i$ are constructed. The accuracy of predicting $\boldsymbol{x}_j$ is then compared between these two models.

$$\boldsymbol{x}_j=\sum_{r=1}^{p}\boldsymbol{A}_j^{(r)}\boldsymbol{X}^{(r)}+\boldsymbol{\varepsilon}_j, \tag{3.2}$$

where $\boldsymbol{x}_j$ represents the j-th row of $\boldsymbol{X}$, $\boldsymbol{A}_j^{(r)}$ represents the j-th row of $\boldsymbol{A}^{(r)}$,

$$\boldsymbol{x}_j=\sum_{r=1}^{p}\boldsymbol{A}_j^{(r)}\boldsymbol{X}^{(r)}+\boldsymbol{\varepsilon}_j, \tag{3.3}$$

where $\boldsymbol{X}^{(r)}=[\boldsymbol{x}_1^{t-1},\boldsymbol{x}_2^{t-r}\cdots\boldsymbol{x}_{i-1}^{t-r},\boldsymbol{x}_{i+1}^{t-r}\cdots\boldsymbol{x}_n^{t-r}]^T$ represents the matrix $\boldsymbol{X}^{(r)}$ with only $\boldsymbol{x}_i$ excluded, and $\boldsymbol{A}_j^{(r)}$ is the corresponding linear dynamics matrix. When the inclusion of $\boldsymbol{x}_i$ aids in more accurately predicting $\boldsymbol{x}_j$ the magnitude of $\boldsymbol{\varepsilon}_j$ will be smaller than that of $\boldsymbol{\varepsilon}_j$. The logarithm of the ratio of the variances of the prediction errors from the two models is defined as the Granger causality from $\boldsymbol{x}_i$ to $\boldsymbol{x}_j$, which is positively correlated with the assistance of $\boldsymbol{x}_i$ in predicting $\boldsymbol{x}_j$,

$$\mathrm{F}_{i\to j}=\ln\frac{var(\tilde{\boldsymbol{\varepsilon}}_j)}{var(\boldsymbol{\varepsilon}_j)}. \tag{3.4}$$

Despite its simplicity and intuitiveness, Granger causality imposes stringent definitions on its applicability. Numerous explicit or implicit assumptions serve as prerequisites for employing Granger causality [29], some of which are restrictive:

- **Temporal Order**: Causality is temporally ordered, with causes preceding effects; instantaneous causality without time delay is not considered.
- **Stationarity**: The statistical properties of data, such as variance and mean, are time-invariant.
- **Linearity**: The interactions between variables are assumed to be linear and can be accurately described by an Auto-Regressive model.
- **Known Time Lag**: The extent to which causality exist in the history of variables is known and is represented by a fixed time lag.
- **Complete System**: It is assumed that the analysis incorporates all relevant variables and that there are no unmeasured confounders

These prerequisites have been designed to ensure the accuracy of Granger causality, thereby avoiding spurious or missing causality. However, they are difficult to fully satisfy in practice. For example, many real-world multivariate time series are non-stationary [30]. Nonlinearity is a common feature of complex dynamical systems, which renders linear models an inadequate tool of accurate description. Moreover, it is difficult to exclude all confounding factors without sufficient prior knowledge. These issues significantly constrain the reasonable application of Granger causality. Researchers must incorporate sufficient prior knowledge and apply Granger causality cautiously. On the other hand, some researchers have proposed improved methods to tackle these issues, such as Lasso-Granger causality and its variants [31-33], nonlinear Granger causality that replaces linear VAR models with RBF models [34], or kernel regressions [35].

4. Modified Granger causality inspired by Galerkin models

The modified Granger causality (MGC), tailored for the Galerkin model, retains the concept and the framework of original method. The following modifications have been made to ensure that the modified method meets the prerequisites and is capable of analyzing the Galerkin model.

- **Nonlinearity:** Fluid systems exhibit a high degree of nonlinearity; research has showed that complex unsteady flows arise from Hopf bifurcations of cubic nonlinearity within the quadratic nonlinear Navier-Stokes equation [36]. Standard Granger causality cannot accurately analyze fluid systems as it does not account for complex nonlinear interactions. To deal with this problem, we keep the linear terms and add all the possible quadratic terms and constant terms to the regression in order to model the body forces and the nonlinear convection.
- **Relaxed stationarity assumption**: Regarding the stationarity assumption, Granger [3] himself described it as, "In the nonstationary case, (variance) will depend on time t and, in general, the existence of causality may alter over time". In other words, stationary sequences have time-invariant variance, which leads to time-invariant Granger causality. However, unsteady flows are highly time-varying, and it is likely that different causal relationships will emerge at different stages of flow development. Thus, the requirement for absolute stationarity of the data is impractical, which is relaxed in the modified Granger causality. Instead, sufficient prior knowledge is used to validate the results of causal analysis, thereby preventing spurious causality.
- **Fixed time lag**: The time lag is a critical parameter in Granger causality, and its selection typically relies on prior knowledge or criteria that balance model accuracy and complexity, such as the Akaike Information Criterion (AIC) [37] and the Bayesian Information Criterion (BIC) [38]. Utilizing the existing knowledge that the Galerkin model comprises a system of first-order differential equations, we set the order of time lag in modified Granger causality to 1. Although higher-order differences can also approximate first-order time derivatives, studies suggest that increasing the order of time lag may lead to overfitting in high-dimensional VAR models [39]. This phenomenon was observed during our own tests, which resulted in unclear causality.

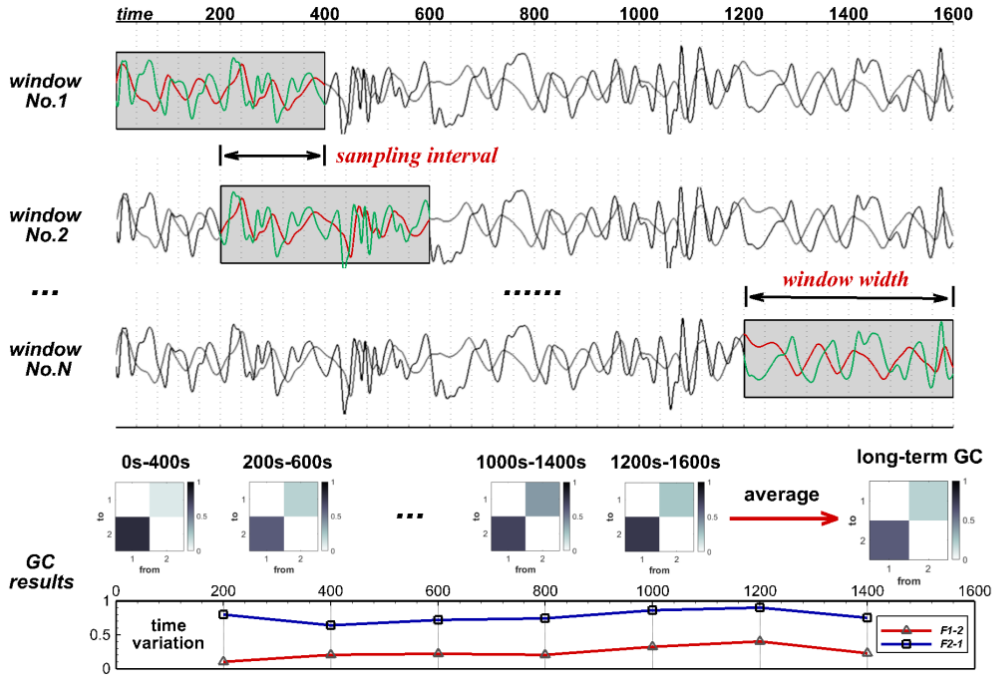

Figure 1. Schematic of segmented sampling for modified Granger causality. The time series of two variables are equidistantly partitioned into intervals, with Granger causality applied to each interval to capture time-varying short-term causality. The results are subsequently ensemble-averaged to derive the long-term causality.

As previously mentioned, the causality in unsteady flows is likely to be time-varying, rendering holistic analysis inadequate to capture the variations. Therefore, the modified Granger causality divides the series into several sampling windows of equal length. Within each sampling window, Granger causality is applied to discover short-term causality, which can characterize the temporal evolution of causality. The ensemble average of these short-term causalities is taken to reflect long-term causality. The segmentation of the series is determined by two parameters: window length and sampling interval. The former indicates the length of each sampling window, while the latter specifies the distance between two consecutive sampling windows. In this study, the sampling interval is simply selected as half of the window length, whereas the window length requires careful selection due to its significant impact on the final results. We found that an insufficient window length may result in inadequate training data, which consequently lead to an inaccurate model and erroneous causality estimation. Conversely, an excessively long window length lacks the resolution necessary to capture short-term causality, which is also unacceptable. In order to determine the window length in a reasonable manner, the following criteria, namely the causal discrimination index (CDI), is defined

$$CDI = \frac{std(\mathrm{F}_{i\to j})}{avg(\mathrm{F}_{i\to j})} = \sqrt{\frac{1}{m-1}\sum_{i,j=1}^{n}\left(\mathrm{F}_{i\to j} - \frac{1}{m}\sum_{i,j=1}^{n}\mathrm{F}_{i\to j}\right)^2}, \quad i \neq j, \tag{3.5}$$

where n denotes the number of modes, $m = \mathrm{C}_n^2$ denotes the number of pairs, $std(\cdot)$ denotes the unbiased standard deviation, and $avg(\cdot)$ represents the mean value. $\mathrm{F}_{i\to j}$ indicates the Granger causality from mode i to mode j. CDI is defined as the root mean square (RMS) of the differences between all causalities and the mean. The desired outcome of causal analysis facilitates distinct differentiation among strong causality, weak causality, and non-causality (as depicted in figure 1), corresponding to a high causal siscrimination index (CDI). Consequently, the selection of the window length is intended to maximize the CDI.

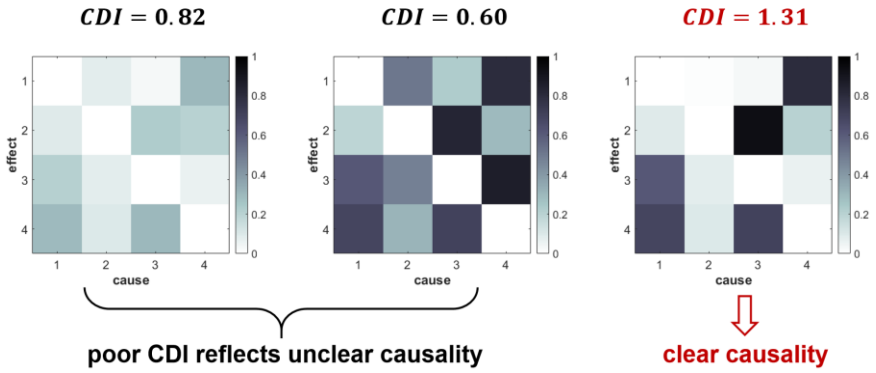

Figure 2. In the three exemplary causality diagrams above, the one on the right is the best, exhibiting the clearest causal structure. The causal discrimination index (CDI) is displayed above each causality diagram, and it is evident that clearest causal structures correspond to highest CDI values.

After the aforementioned modifications, the modified Granger causality (MGC) is defined as follows. Consider a Galerkin model composed of n modes ($x_1, x_2, x_3, \cdots x_n$). First, an appropriate window length is selected to segment the modal coefficient series into several equally spaced sampling windows. To evaluate the causal effect $\mathrm{F}_{p\to q}$, a full model that uses all modes to predict mode q is constructed in each sampling window

$$\boldsymbol{x}_q = \sum_{i=1}^{n} a_i \boldsymbol{x}_i^{(1)} + \sum_{i,j=1,\, i\le j}^{n} b_{ij}\boldsymbol{x}_i^{(1)}\boldsymbol{x}_j^{(1)} + c + \boldsymbol{\varepsilon}_q, \tag{3.6}$$

where $\boldsymbol{x}_q$ is the coefficient vector of mode q. $a_i\boldsymbol{x}_i^{(1)}$ represents the linear regression term, with the

superscript (1) indicating the order of the time lag is 1. $b_{ij}\boldsymbol{x}_i^{(1)}\boldsymbol{x}_j^{(1)}$ denotes the quadratic regression term, $\mathcal{C}$ is the constant term, and $\boldsymbol{\varepsilon}_q$ is the prediction error. Subsequently, by excluding all linear and quadratic terms involving mode p, the reduced model is constructed

$$\boldsymbol{x}_q = \sum_{i=1}^{n} a_i \boldsymbol{x}_i^{(1)} + \sum_{i,j=1,i\le j}^{n} b_{ij}\boldsymbol{x}_i^{(1)}\boldsymbol{x}_j^{(1)} + \tilde{c} + \boldsymbol{\varepsilon}_q, \quad (i,j \neq p). \tag{3.7}$$

The constraint $i, j \neq p$ in the reduced model excludes all terms involving mode p, and $\boldsymbol{\varepsilon}_q$ is the error vector. In accordance with the classical Granger causality, $\mathrm{F}_{p\to q}$ in each sampling interval is defined as the logarithm of the ratio of two variances

$$\mathrm{F}_{p\to q}^{\,k} = \ln \frac{var(\boldsymbol{\varepsilon}_q)}{var(\boldsymbol{\varepsilon}_q)}, \quad k = 1,2,3,\cdots n, \tag{3.8}$$

where $var(\boldsymbol{\varepsilon})$ denotes the variance of the error vector. By repeating the analysis in all sampling windows, the short-term causality within each sampling window can be obtained, characterizing the variation of causality throughout the flow evolution. Taking the average of the results from all sampling windows, the long-term causality of the entire sequence is finally obtained

$$\mathrm{F}_{p\to q} = \frac{1}{n}(\mathrm{F}_{p\to q}^{\,-1} + \mathrm{F}_{p\to q}^{\,-2} + \mathrm{F}_{p\to q}^{\,-3} \cdots + \mathrm{F}_{p\to q}^{\,-n}). \tag{3.9}$$

5. Application

In this chapter, the effectiveness of the proposed modified Granger causality (MGC) is demonstrated through the application to a 9-equation turbulent shear flow model [40]. We analyzed causal relationships between modes using both knowledge-based method and the data-driven method (modified Granger causality). The results reveal high consistency in the causalities identified by the two approaches. Specifically, the knowledge-based framework offers deeper insights into the physical mechanisms, whereas the modified Granger causality quantifies causal strength through statistical significance. By combining these methods, we harness their respective strengths: the qualitative insights from knowledge-based analysis and the quantitative outcomes from data-driven analysis. Furthermore, by employing a segmented sampling strategy, we investigate the temporal evolution of causality within turbulent shear flow. We demonstrated that the identified causality can guide flow control, thereby validating the practical utility of this causal analysis framework.

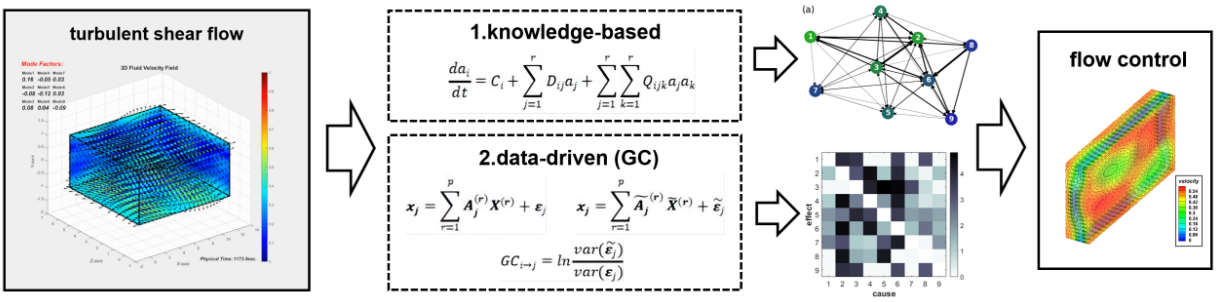

Figure 3. Application of knowledge-based and data-driven causal analysis in the model of turbulent shear flow

5.1. Nine-equation turbulent shear flow model

Turbulence remains a significant challenge in fluid mechanics due to its inherent complexity and strong nonlinearity. In 1997, Waleffe [19] proposed a reduced-order model for turbulent shear flows based on Galerkin projection, which included eight Fourier velocity modes. In 2004, Moehlis et al. introduced a mean flow correction mode, extending the framework to develop a refined nine-equation turbulent shear flows model.

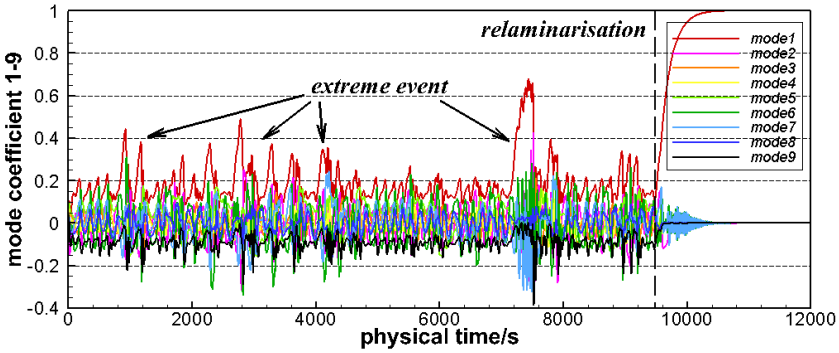

Figure 4. Temporal evolution of mode coefficients in turbulent shear flow model. Extreme events (indicated by black arrows) punctuate the transitional dynamics, with the system decaying to a steady shear flow state after 10,000 seconds.

The model depicts three-dimensional shear flow turbulence induced by sinusoidal body forcing [40]. The velocity is broken down into nine Fourier velocity modes: the base profile (mode 1), streak (mode 2), downstream vortex (mode 3), spanwise flow (modes 4 and 5), normal vortex (modes 6 and 7), fully three-dimensional structure (mode 8), and modification of the base profile (mode 9). By projecting the incompressible Navier-Stokes equations onto these nine velocity modes, a system of ordinary differential equations is derived (see Appedix A.).

Table 1. Parameter setting for the turbulent shear flow model

Parameter	Explanation	Value
Lx	length of the domain in the x direction	4π
Ly	length of the domain in the y direction	1
Lz	length of the domain in the z direction	2π
Re	Reynolds number	400
dt	integration time step	0.1s
Time	total time of the evolution	12000s
Initial condition	$(a_1, a_2, a_3 \cdots a_9) = (0,\ 0.1,\ 0.1,\ 0.1,\ 0.1,\ 0,\ 0,\ 0,\ 0)$	

The system of ordinary differentia] equations is numerically integrated using a fourth-order Runge-Kutta scheme with parameters specified in table 1. As illustrated in figure 4, the temporal evolution of modal coefficients exhibits chaotic flow dynamics, ultimately decaying to a steady state. Throughout the transition phase, intermittent bursts of intense variations are observed, notably characterized by the rapid growth of mode 1 coefficients, signaling tendencies towards relaminarization. These transient bursts are defined as extreme events in turbulent systems [41]. Owing to its minimalist formulation and its ability to model fundamental turbulence features—including multiscale fluctuations, energy dissipation, and relaminarization dynamics—this model has become a benchmark for studying transitional flows [42], turbulence modelling [43], and control of extreme events [44].

5.2. Knowledge-based causal analysis

Utilizing the mathematical and physical principles of Galerkin projection as background knowledge, we qualitatively analyzed the causal relationships between modes. The four basic physical mechanisms within the model were identified, and their resulting causal relationships were examined:

- **Body Force:** The constant term in the equation of mode 1 represents energy injection into the flow by external body forces. This mechanism does not entail causality between modes.
- **Viscous Dissipation:** Each mode's equation comprises a first-order term with a coefficient that is nearly, but slightly less than one, representing viscous dissipation which causes exponential decay in mode amplitudes. This mechanism does not entail causality between modes.

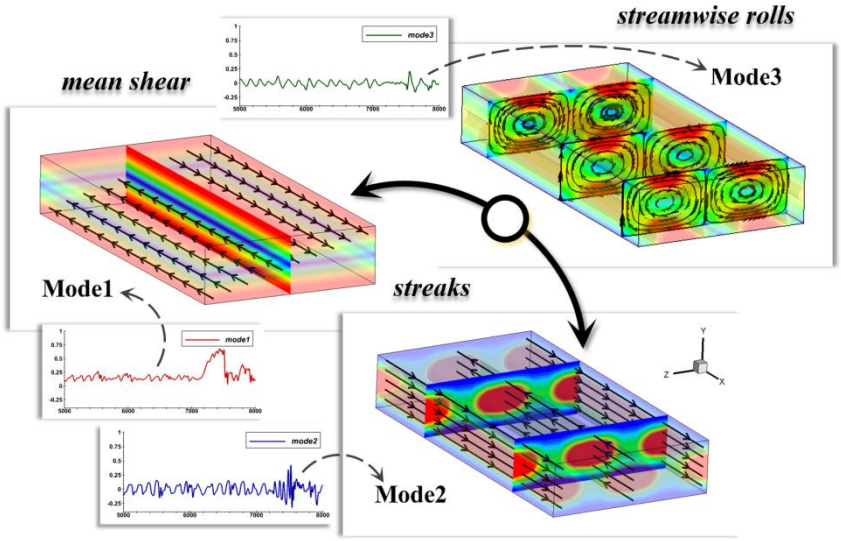

Figure 5. Conversion between main shear (mode 1) and streaks (mode 2), modulated by the streamwise rolls (mode 3). Three-dimensional mode contours and the temporal evolution of mode coefficients are depicted.

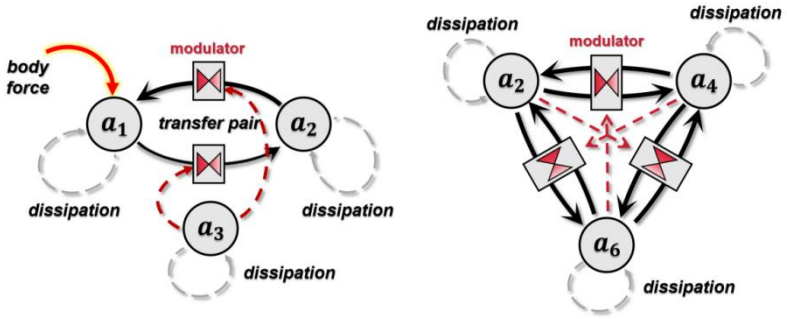

Figure 6. Two types of modal interaction. left: Modulated Two-mode coupling; right:Triad interactions

- **Modulated two-mode coupling:** This mechanism is characterized by the mutual conversion of two modes controlled by a third mode, whose evolution remains independent of the other two. For instance, consider the system within mode 1, mode 2 and mode 3. It can be seen that the differential equations of mode 1 and mode 2 contain quadratic terms with coefficients of opposite signs (e.g. $Q_{123} = Q_{213} \neq 0$), while mode 3 lacks terms involving mode 1 or mode 2 ($Q_{312} = 0$). We can conclude that mode 1 and mode 2 form a **transfer pair**, with Mode 3 acting as a catalyst that facilitates their interaction without direct feedback, defined as **modulator**. As illustrated in figure 5, this relationship physically represents a self-sustaining process (SSP) in shear flows where streamwise rolls redistribute the mean shear to create streaks [19]. Such interactions are

denoted as $[a_1 \square a_2]a_3$, with analogous instances including $[a_1 \square a_6]a_8$, $[a_4 \square a_5]a_1$ et al. This configureuration consists of four causal relations: a bidirectional interaction within the transfer pair and two unidirectional connections from the modulator to each member of the transfer pair.

- **Triad interactions:** This mechanism involves mutual coupling among three modes, where each mode acts as a modulator for the conversion of the other two modes. It was first identified by Kraichnan and Chen [45] in 1989. In the turbulent shear flow model, mode 2, mode 4, and mode 6 form a triad interaction, appearing in each other's evolution equations with quadratic term coefficients that strictly sum to zero ($Q_{246}+Q_{426}+Q_{624}=0$). This configureuration ensures mutual energy transfer between modes while conserving the total energy [46,47], as illustrated in figure 6 (right). Such relationships are denoted as $\mathrm{T}(a_2,a_4,a_6)$ with analogous instances including $\mathrm{T}(a_3,a_5,a_6)$ and $\mathrm{T}(a_3,a_4,a_7)$. Within triad interactions, each pair of modes exhibits bidirectional causality, resulting in six causal relations.

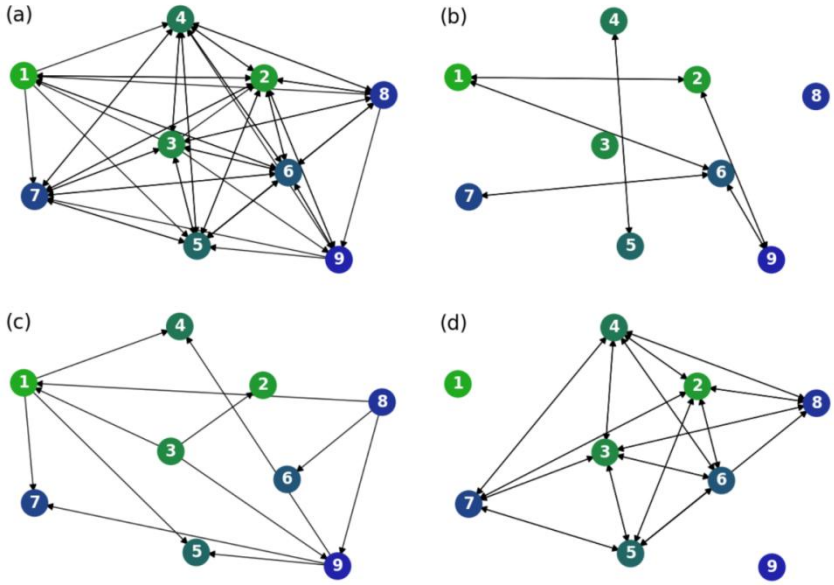

Figure 7. Causal network among turbulent shear flow modes derived from knowledge-based analysis. Single arrows denote unidirectional causality from "cause" to "effect" modes, while double arrows indicate bidirectional causalities. a) The summation of all causalities; b) Causalities between transfer pairs; c) Causalities from the modulator to the transfer pair; d) Causalities of triad interactions

Table 2. Summary of identified mechanisms in turbulent shear flow model

Physical mechanism	**Instance**
Body force	acting on mode 1
Dissipation	acting on all modes
Modulated two-mode coupling	$[a_1 \square a_2]a_3$, $[a_2 \square a_9]a_3$, $[a_1 \square a_6]a_8$, $[a_6 \square a_9]a_8$, $[a_4 \square a_5]a_1$, $[a_4 \square a_5]a_9$, $[a_6 \square a_7]a_1$, $[a_6 \square a_7]a_9$

Triad interactions	$\mathrm{T}(a_2,a_4,a_6)$, $\mathrm{T}(a_2,a_5,a_7)$, $\mathrm{T}(a_2,a_5,a_8)$, $\mathrm{T}(a_3,a_5,a_6)$, $\mathrm{T}(a_3,a_4,a_7)$, $\mathrm{T}(a_3,a_4,a_8)$

Here, causality is defined as direct interactions between modes. The absence of causality does not preclude the possibility of indirect interactions, which may occur through intermediate modes. We summarize the physical mechanisms identified in the turbulent shear flow model in table 2. All identified causal relationships are displayed in a directed graph in figure 7. Among the 9 modes, there are 56 actual causal connections (figure 7(a)), including 12 within transfer pairs (figure 7(b)), 14 from modulators to transfer pairs (figure 7(c)), and 32 arising from triad interactions (figure 7(d)). Notably, $a_1 \leftrightarrow a_6$ and $a_6 \leftrightarrow a_9$ exhibit dual causality, encompassing both bidirectional causality within transfer airs aPnd unidirectional causality from modulators to transfer pairs. The knowledge-based causal analysis, rooted in mathematical and physical principles, yields highly accurate and reliable results. However, its inability to quantify causal strength is a notable limitation. However, data-driven method can provide quantitative capabilities, as will be demonstrated in the following section.

5.3. Data-Driven Causal Analysis

The modified Granger causality (MGC) was applied to analyze data generated using the parameters specified in table 1. To determine the optimal window length, the relationship between prediction error (defined as the root mean square error (RMSE) of mode coefficients), causal discrimination index (CDI), and sampling length was investigated, as illustrated in figure 8. The sampling window length was ultimately set to 400 seconds, corresponding to the maximum CDI and a stabilized prediction error. This choice ensures sufficient model accuracy while maximizing the causal resolution among strong causality, weak causality, and non-causality.

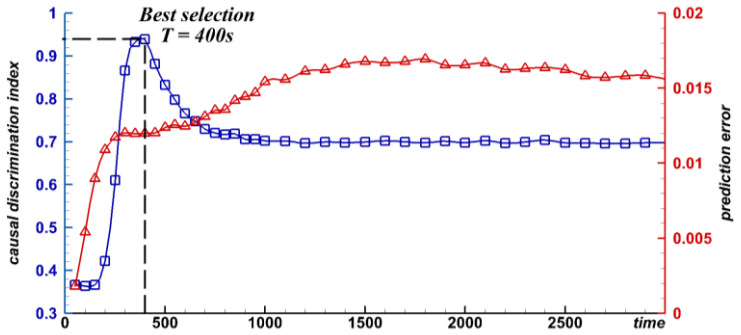

Figure 8. The variation of the causal discrimination index (blue curve) and model prediction error (red curve) as functions of sampling length. The optimal window length (T=400s) strikes a balance between causal resolution and model accuracy.

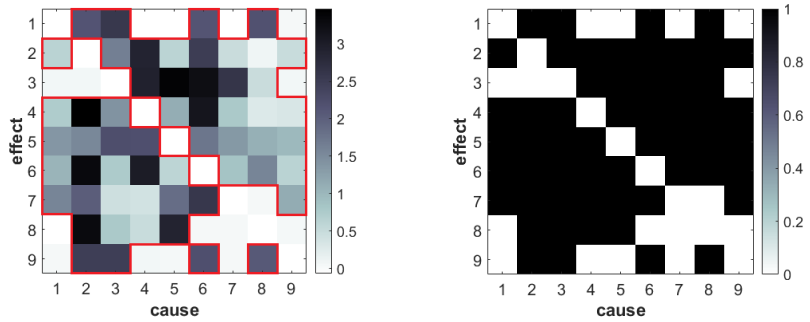

Figure 9. Comparison of causal maps derived from data-driven (left: modified Granger causality) and knowledge-based (right: Section 5-2) methods. Causality identified by the knowledge-based method is demarcated with red boxes.

The results of data-driven and knowledge-based causal analysis are compared in figure 9. Notably, regions exhibiting stronger modified Granger causality (MGC) align closely with these identified by knowledge-based method. However, exclusive reliance on MGC risks misclassifying weak causal interactions (e.g. $a_8 \rightarrow a_2$) as non-causal. The knowledge-based framework rectifies such ambiguities by integrating physical information, as exemplified by its identification of causality from mode 8 to mode 2 despite low MGC values. This hybrid approach ensures robust causal inference.

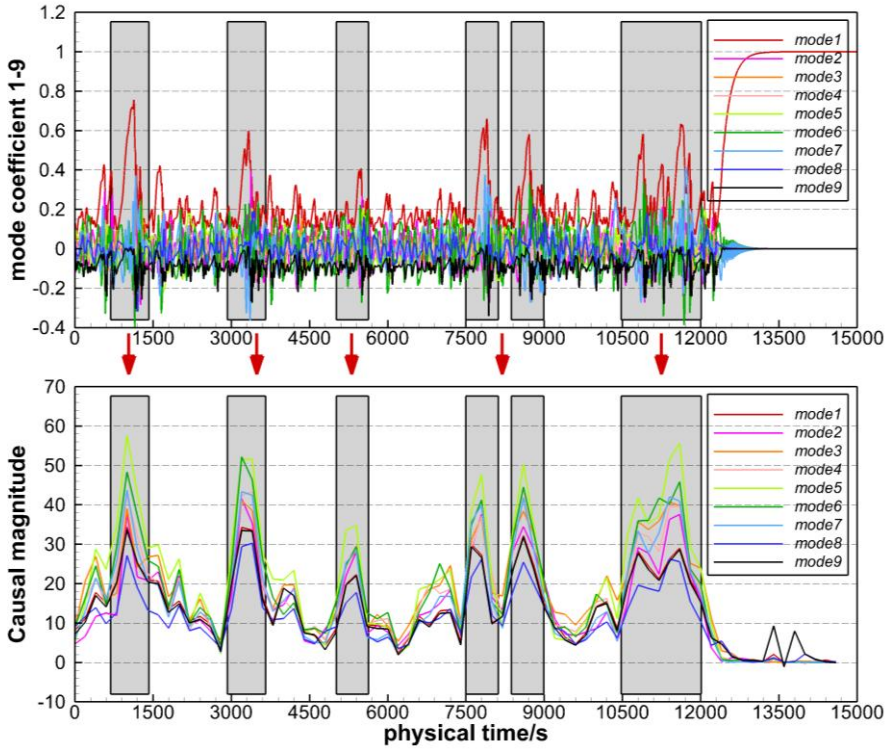

Figure 10. Variation in causal magnitude with turbulence development. The upper panel shows the evolution of the mode coefficients, while the lower panel illustrates the variation of the causal magnitude. The gray boxes highlight the extreme events in the turbulence, which correspond to sharp rises in causal magnitude.

In addition to quantifying the strength of causal relationships, the modified Granger causality can also analyze the dynamic variations in causality. By examining how causality varies with turbulent fluctuations, a strong correlation between the magnitude of Granger causality and extreme events is observed. To quantify the causal magnitude at a specific instant in the flow, the causal strength of one mode on all other modes is summed

$$CM_i = \sum_{i=1}^{n} \mathrm{F}_{i \rightarrow j}, \tag{4.1}$$

where n represents the number of modes. Using a segmented sampling strategy with a sampling length of $T = 400s$, we investigated the evolution of causal magnitude for each mode as turbulence developed. A large range of sequences was analyzed, and a typical one is shown in figure 10. Within the gray box, an extreme event occurs, characterized by a sharp rise in the mode 1 coefficient. Simultaneously, the causal magnitude of all modes increases sharply. This phenomenon indicates that the occurrence of extreme events leads to an enhancement of causality.

Subsequently, the differences between the modified Granger causality and the classical Granger causality are compared. By varying the initial conditions, Reynolds number, and sampling window length, we obtaine four sets of data samples. These samples are analyzed using the modified Granger

causality, the classical Granger causality (implemented with the MVGC toolbox developed by Barnett and Seth [48]), and Pearson correlation to examine the causal relationships between modes. The results are shown in figure 11. We observe significant variations in the results of classic Granger causality across the four datasets, indicating its deficiency in robustness. This shows that the classical Granger causality, as a linear method, is unreliable for evaluating causality in nonlinear systems. In contrast, the modified Granger causality produced highly consistent results across all datasets, demonstrating strong robustness. It confirms that our modifications to the Granger causality method are both reasonable and effective. Although Pearson correlation also yielded robust results, it only reflects similarities in the trends of variation between mode coefficient, not causality. For instance, mode 1 and mode 9, as well as mode 2 and mode 3, exhibit high similarity, but this does not imply a causal relationship between them. These results underscore the fundamental distinction between causality and correlation.

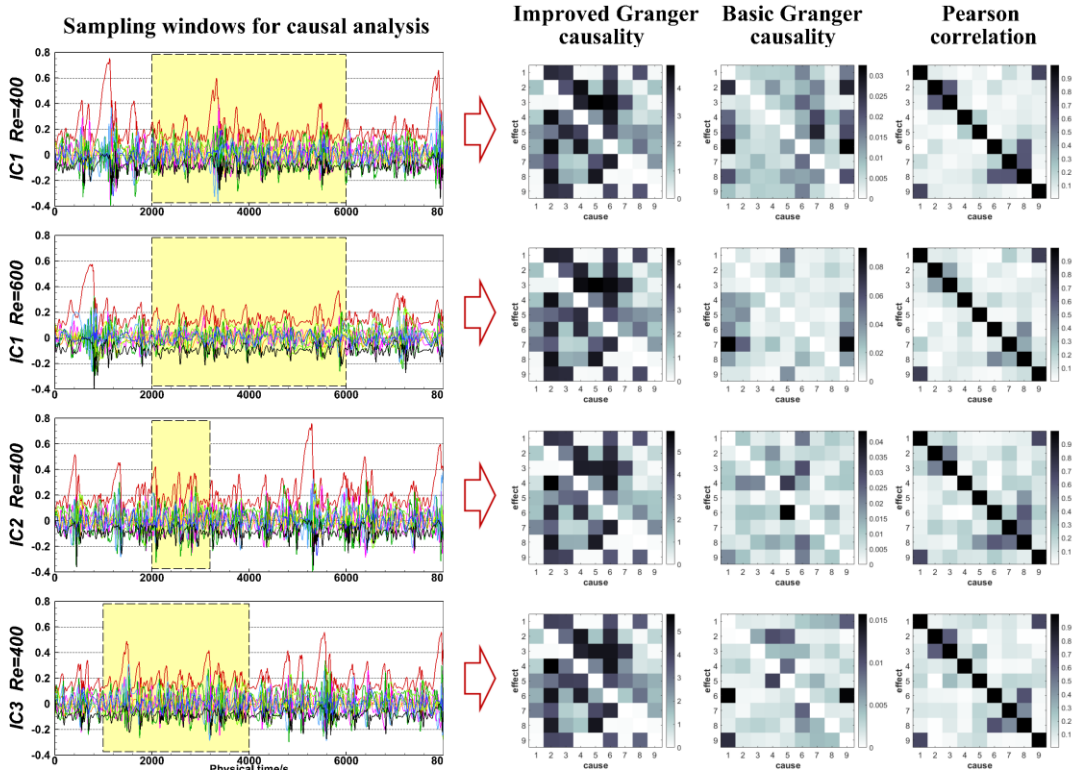

Figure 11. Comparison of modified Granger causality, classical Granger causality, and Pearson correlation. Four distinct modal evolution sequences are presented on the left, each corresponding to a unique set of initial conditions and Reynolds numbers. The yellow boxes denote the sampling windows. The results obtained from the three methods are displayed sequentially on the right.

5.4. Application of Causal Analysis: Suppression of Extreme Events

This section demonstrates how causal analysis can deepen our understanding of flow mechanisms, offering valuable insights for flow control strategies. At low Reynolds numbers, the turbulent shear flow exhibits significant instability, with extreme events emerging when viscous dissipation and externally applied periodic body forces dominate. Racca and Magri [44] employed Echo State Networks (ESN) to predict the evolution of mode coefficients and successfully suppressed extreme events by artificially increasing the Reynolds number prior to their onset. Inspired by their work, we propose a simple but effective flow control approach from a causal perspective.

The rapid growth of mode 1 is a dominant characteristic of extreme events.; thus, suppressing these events hinges on effectively regulating mode 1. As previously analyzed, mode 1 forms transfer pairs with modes 2 and 3, and modes 6 and 8, respectively (as illustrated in figure 5 and figure 6). Consequently, the onset of extreme events is attributed to the rate of energy injection by body forces exceeding the rate of energy transfer from mode 1 to modes 2 and 6, resulting in energy accumulation

in mode 1. Building on this insight, we propose the following flow control strategy. Consider the transfer pair composed of mode 1, mode 2, and mode 3. In circumstances where mode 1 exhibits a rapid growth trend, an artificial body force is applied to mode 3 (the modulator) in either a positive or negative direction, thereby facilitating the transfer of energy from mode 1 to mode 2 to suppress the growth of mode 1.

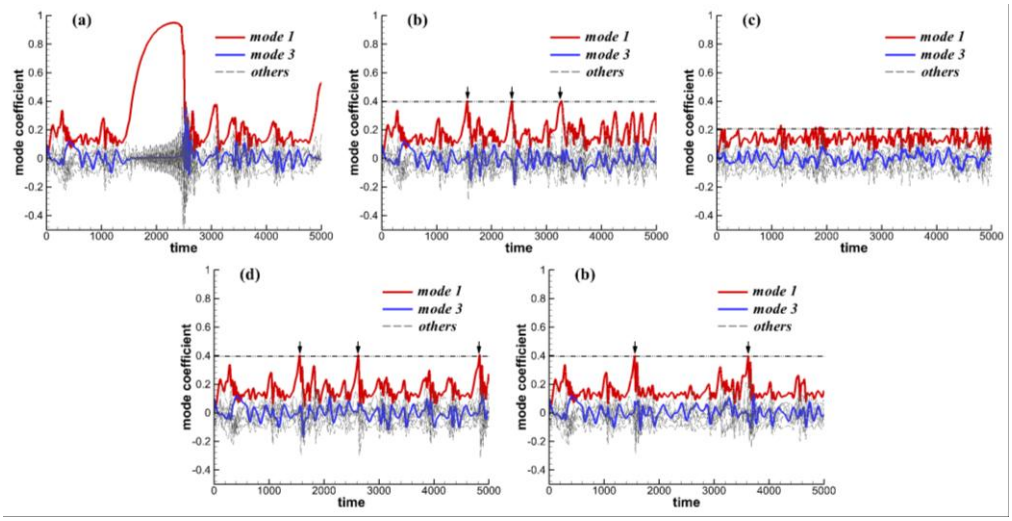

Figure 12. Suppression of extreme events by applying body force to mode 3 under the condition $\boldsymbol{a}_0 = (0,\ 0.03,\ 0.1,\ 0.05,\ 0.1,\ 0,\ 0,\ 0.04,\ 0),\ \mathrm{Re} = 600$. In (a)-(c), the time step is 0.1s, and the perturbation amplitude is 0.01. (a) shows the evolution of modes without control, while (b) and (c) present the control results with thresholds set at 0.4 and 0.2, respectively. Compared to the conditions in (b), the time step for (d) is reduced to 0.01s, and the perturbation amplitude for (c) is increased to 0.1. The interval at which control takes effect is marked by the small black arrows.

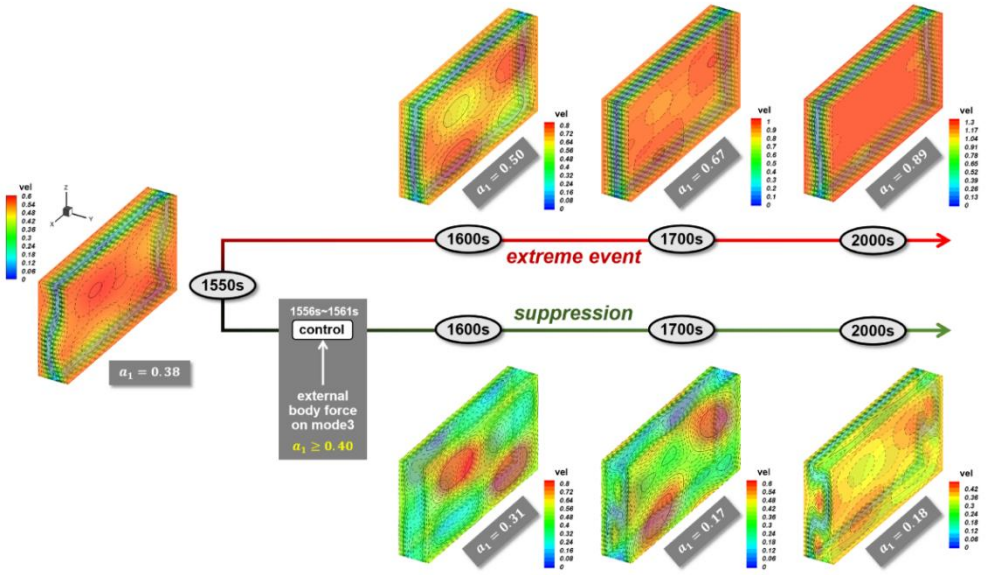

Figure 13. Comparison of flow contours before and after control. The upper and lower tracks display flow contours at 1550s, 1600s, 1700s, and 2000s from figure 16(a) and 16(b), respectively. The control system for suppressing extreme events detects whether the coefficient of mode 1 exceeds the threshold of 0.4 and is activated between 1556s and 1561s.

The flow control algorithm is governed by three parameters: threshold, perturbation amplitude and time step, which is described in Algorithm 1. To ensure that the intervention consistently suppresses the growth of mode 1, the direction of body force is controlled based on the sign of mode 2, formulated as

$$f = -p \cdot sgn(a_2) \cdot \mathrm{ReLU}(a_1 - a_{\mathrm{TH}}), \tag{4.2}$$

where p represents the perturbation amplitude, $sgn(\cdot)$ denotes the sign function, and $\mathrm{ReLU}(\cdot)$ refers to the linear rectification function.

Algorithm 1: Algorithm to suppress extreme event through mode 3

parameters:

- Threshold $a_{TH} \in (0.1,1)$: threshold for control operation
- Perturbation amplitude $p \in (0.001,1)$: magnitude of artificial body force
- Time step $dt \in (0,0.1)$: time step for observation and control

apply artificial body force on mode 3,

i.e. replace $\frac{da}{dt} = \mathrm{N}\ (a_1, a_2 \ldots a_9)$ with $\frac{da}{dt} = \mathrm{N}\ (a_1, a_2 \ldots a_9) - f$

while true

if $a > a_{TH}$

control in effect, $f = -p \cdot sgn(a_2) \cdot (a - a_{TH})$.

else

no control, $f = 0$.

end if

turbulence evolves one time step dt .

end while

With a time step of 0.1 and a perturbation amplitude of 0.1, the control system consistently ensures effective suppression of extreme events under various initial conditions and thresholds, as illustrated in figure 12(a)-(c). Further testing reveals that modifying the time step and perturbation amplitude influences the response speed of the control system, thereby affecting the evolution of the flow, as shown in figure 12(d)-(e). Despite these variations, the system remains capable of effectively suppressing extreme events, demonstrating strong robustness. The operational time of the control system is notably brief, minimizing both control costs and flow interference. The flow fields before and after suppressing extreme events are depicted in figure 13. It is clear that the activation of the control system induces a significant transformation in the flow structure, effectively halting the transition of turbulence into steady shear flow.

6. Conclusion

Causal analysis in fluid mechanics is an emerging and promising research approach with significant potential for application. While existing studies have utilized data-driven algorithms to discover causal relationships in complex flows, concerns regarding the interpretability and reliability of such approach still persist. In this work, we address these limitations by integrating both knowledge-based and data-driven causal analysis, proposing a hybrid framework tailored for Galerkin models. The knowledge-based analysis utilizes the mathematical and physical principles inherent in Galerkin models, while the data-driven analysis employs a modified Granger causality that exhibits improved robustness and accuracy compared to the classic method. We validated the effectiveness of this hybrid approach using a 9-equation turbulent shear flow model [40]. The knowledge-based component of the framework identified two distinct types of modal interactions: transfer pairs between two modes and triad interactions among three modes. Causalities within these interactions were qualitatively characterized by

the knowledge-based analysis. Subsequently, it is shown that the identified causality from knowledge is also characterized by the data-driven analysis, which further quantified the strength of these causal relationships and captured their temporal variations. Building on these insights, we implemented causality-guided flow control by applying intermittent body forces to specific modes, effectively suppressing extreme events in the turbulent shear flow. This demonstrates how causality can be applied in practice.

The contributions of this work are threefold. First, we introduce a hybrid causal analysis framework that combines knowledge-based and data-driven methodologies. This framework utilizes existing knowledge and data to identify causal mechanisms within complex flows, while cross-validation between the two approaches enhances the interpretability and reliability of the identified causality. Second, we develop an improved Granger causality specifically designed for Galerkin models. The incorporation of quadratic terms into the method enables the capture of nonlinear interactions, thereby enhancing both accuracy and robustness. Furthermore, a segmented sampling strategy and causal discrimination index (CDI) is introduced, which facilitates the detection of temporal variations in causalities. Thirdly, the practical value of causality is demonstrated through causality-guided flow control. Based on causality, the energy transfer mechanisms among modes were elucidated, thus enabling the design of an efficient flow control system.

Currently, the proposed hybrid framework is specifically tailored for Galerkin models. Extending this approach to other low-dimensional models (ROMs) remains an open challenge. Two primary obstacles must be addressed. First, the framework's reliance on prior knowledge limits its applicability to systems where such knowledge is scarce, such as black-box models constructed using neural networks. Second, the adaptability of the data-driven causal analysis algorithm needs to be enhanced. While the modified Granger causality proposed here is theoretically applicable to ROMs with second-order nonlinearities, its generalization to other systems may require dynamic adjustments. Future research may focus on overcoming these limitations and developing causal analysis frameworks capable of analyzing a broader range of models. With advancements in computational resources, the direct causal analysis of high-dimensional flows may also become feasible. Such an approach would preserve the intricate details of the flow, offering deeper insights into microscopic causal mechanisms.

Appendix A.

The system of ordinary differential equations (ODE) derived from the 9-equation turbulent shear flow model are presented below. For further information on this model, please refer to [40].

$$\frac{da_1}{dt} = \frac{\beta^2}{Re} - \frac{\beta^2}{Re} a_1 - \sqrt{\frac{3}{2}} \frac{\beta y}{k_{a\beta y}} a_6 a_8 + \sqrt{\frac{3}{2}} \frac{\beta y}{k_{\beta y}} a_2 a_3, \tag{A.1}$$

$$\frac{da_2}{dt} = -\left(\frac{4\beta^2}{3} + \gamma^2 \right) \frac{a_2}{Re} + \frac{5\sqrt{2}}{3\sqrt{3}} \frac{\gamma^2}{k_{a\gamma}} a_4 a_6 - \frac{\gamma^2}{\sqrt{6k_{a\gamma}}} a_5 a_7 - \frac{\alpha\beta y}{\sqrt{6k_{a\gamma}} k_{a\beta y}} a_5 a_8 \tag{A.2}$$

$$\frac{da_3}{dt} = -\frac{\beta^2 + \gamma^2}{Re} a_3 + \frac{\beta^2(3\alpha^2 + \gamma^2) - 3\gamma^2(\alpha^2 + \gamma^2)}{\sqrt{6k_{a\gamma} k_{\beta y} k_{a\beta y}}} a_4 a_8, \tag{A.3}$$

$$\frac{da_4}{dt} = -\frac{3\alpha^2+4\beta^2}{3Re}a_4 - \frac{10}{3\sqrt{6}}\frac{\alpha^2}{k_{a\gamma}}a_2a_6 - \sqrt{\frac{3}{2}}\frac{\alpha\beta y}{k_{a\gamma}k_{\beta y}}a_3a_7 - \sqrt{\frac{3}{2}}\frac{\alpha^2\beta^2}{k_{a\gamma}k_{\beta y}k_{a\beta y}}a_3a_8 - \frac{\alpha}{\sqrt{6}}a_1a_5 - \frac{\alpha}{\sqrt{6}}a_5a_9. \tag{A.4}$$

$$\frac{da_6}{dt} = -\frac{3\alpha^2+4\beta^2+3\gamma^2}{3Re}a_6 + \frac{\alpha}{\sqrt{6}}a_1a_7 + \sqrt{\frac{3}{2}}\frac{\beta\gamma}{k_{a\beta\gamma}}a_1a_8 + \frac{10}{3\sqrt{6}}\frac{\alpha^2-\gamma^2}{k_{a\gamma}}a_2a_4 \tag{A.5}$$

$$\frac{da_6}{dt} = -\frac{3\alpha^2+4\beta^2+3\gamma^2}{3Re}a_6 + \frac{\alpha}{\sqrt{6}}a_1a_7 + \sqrt{\frac{3}{2}}\frac{\beta\gamma}{k_{a\beta\gamma}}a_1a_8 + \frac{10}{3\sqrt{6}}\frac{\alpha^2-\gamma^2}{k_{a\gamma}}a_2a_4 + 2\sqrt{\frac{2}{3}}\frac{\alpha\beta\gamma}{k_{a\gamma}k_{\beta\gamma}}a_3a_5 + \frac{\alpha}{\sqrt{6}}a_7a_9 + \sqrt{\frac{3}{2}}\frac{\beta\gamma}{k_{a\beta\gamma}}a_8a_9, \tag{A.6}$$

$$\frac{da_7}{dt} = -\frac{\alpha^2+\beta^2+\gamma^2}{Re}a_7 - \frac{\alpha}{\sqrt{6}}(a_1a_6 + a_6a_9) + \frac{1}{\sqrt{6}}\frac{\gamma^2-\alpha^2}{k_{a\gamma}}a_2a_5 + \frac{1}{\sqrt{6}}\frac{\alpha\beta\gamma}{k_{a\gamma}k_{\beta\gamma}}a_3a_4, \tag{A.7}$$

$$\frac{da_8}{dt} = -\frac{\alpha^2+\beta^2+\gamma^2}{Re}a_8 + \frac{2}{\sqrt{6}}\frac{\alpha\beta\gamma}{k_{a\gamma}k_{a\beta\gamma}}a_2a_5 + \frac{\gamma^2(3\alpha^2-\beta^2+3\gamma^2)}{\sqrt{6}k_{a\gamma}k_{\beta\gamma}k_{a\beta\gamma}}a_3a_4, \tag{A.8}$$

$$\frac{da_9}{dt} = -\frac{9\beta^2}{Re}a_9 + \sqrt{\frac{3}{2}}\frac{\beta\gamma}{k_{\beta\gamma}}a_2a_3 - \sqrt{\frac{3}{2}}\frac{\beta\gamma}{k_{a\beta\gamma}}a_6a_8. \tag{A.9}$$

References

[1] Gustau Camps-Valls, Andreas Gerhardus, Urmi Ninad, Gherardo Varando, Georg Martius, Emili Balaguer-Ballester, Ricardo Vinuesa, Emiliano Diaz, Laure Zanna, Jakob Runge, 'Discovering causal relations and equations from data', Phys. Rep., vol. 1044, pp. 1–68, 2023. DOI: 10.1016/j.physrep.2023.10.001

[2] Á. Martínez-Sánchez, G. Arranz, A. Lozano-Durán, 'Decomposing causality into its synergistic, unique, and redundant components', Nat. Commun., vol. 15, no. 1, pp. 9296, 2024. DOI: 10.1038/s41467-024-48973-z

[3] C. W. J. Granger, 'Investigating causal relations by econometric models and cross-spectral methods', Econometrica, vol. 37, no. 3, pp. 424–438, 1969.

[4] G. Tononi, O. Sporns, 'Measuring information integration', BMC Neurosci., vol. 4, pp. 1–20, 2003. DOI: 10.1186/1471-2202-4-1

[5] T. Schreiber, 'Measuring information transfer', Phys. Rev. Lett., vol. 85, no. 2, pp. 461, 2000. DOI: 10.1103/PhysRevLett.85.461

[6] Andrés Cremades, Sergio Hoyas, Rahul Deshpande, Pedro Quintero, Martin Lellep, Will Junghoon Lee, Jason P. Monty, Nicholas Hutchins, Moritz Linkmann, Ivan Marusic, Ricardo Vinuesa, 'Identifying regions of importance in wall-bounded turbulence through explainable deep learning', Nat. Commun., vol. 15, no. 1, pp. 3864, 2024. DOI: 10.1038/s41467-024-48175-7

[7] G Tissot, A Lozano-Durán, L Cordier, J Jiménez, BR Noack, 'Granger causality in wall-bounded turbulence', J. Phys.: Conf. Ser., vol. 506, no. 1, pp. 012006, 2014. DOI: 10.1088/1742-6596/506/1/012006

[8] A. Lozano-Durán, H. J. Bae, M. P. Encinar, 'Causality of energy-containing eddies in wall turbulence', J. Fluid Mech., vol. 882, pp. A2, 2020. DOI: 10.1017/jfm.2020.2

[9] Á Martínez-Sánchez, E López, S Le Clainche, A Lozano-Durán, A Srivastava, R Vinuesa, 'Causality analysis of large-scale structures in the flow around a wall-mounted square cylinder.' J. Fluid Mech., vol. 967, pp. A1, 2023. DOI: 10.1017/jfm.2023.423

[10] A Lozano-Durán, NC Constantinou, MA Nikolaidis, M Karp, 'Cause-and-effect of linear mechanisms sustaining wall turbulence', J. Fluid Mech., vol. 914, pp. A8, 2021. DOI: 10.1017/jfm.2021.8

[11] A. Lozano-Durán, G. Arranz, 'Information-theoretic formulation of dynamical systems: causality, modeling, and control', Phys. Rev. Res., vol. 4, no. 2, pp. 023195, 2022. DOI: 10.1103/PhysRevResearch.4.023195

[12] J. Jiménez, 'Machine-aided turbulence theory', J. Fluid Mech., vol. 854, pp. R1, 2018. DOI: 10.1017/jfm.2018.854

[13] M. P. Encinar, J. Jiménez, 'Identifying causally significant features in three-dimensional isotropic turbulence', J. Fluid Mech., vol. 965, pp. A20, 2023. DOI: 10.1017/jfm.2023.20

[14] P Zhang, M Rosen, SD Peterson, M Porfiri, 'An information-theoretic approach to study fluid–structure interactions', J. Fluid Mech., vol. 848, pp. 968–986, 2018. DOI: 10.1017/jfm.2018.848
[15] S Bagchi, VR Unni, A Saha, 'Transition to Limit-Cycle Oscillation in Fluid-Structure Interactions: Mutual Correlations and Causal Dependencies', AIAA J., vol. 61, no. 4, pp. 1475–1484, 2023. DOI: 10.2514/1.J061475
[16] N. Omata, S. Tsutsumi, 'Causal Analysis of Flowfields Using Clustering Entropy', AIAA J., vol. 58, no. 12, pp. 5472–5477, 2020. DOI: 10.2514/1.J0585472
[17] D. A. Smirnov, 'Spurious causalities with transfer entropy', Phys. Rev. E, vol. 87, no. 4, pp. 042917, 2013. DOI: 10.1103/PhysRevE.87.042917
[18] P. A. Stokes, P. L. Purdon, 'A study of problems encountered in Granger causality analysis from a neuroscience perspective', Proc. Natl. Acad. Sci., vol. 114, no. 34, pp. E7063–E7072, 2017. DOI: 10.1073/pnas.1708273114
[19] F. Waleffe, 'On a self-sustaining process in shear flows', Phys. Fluids, vol. 9, no. 4, pp. 883–900, 1997. DOI: 10.1063/1.869199
[20] I. Akhtar, 'Parallel simulations, reduced-order modeling, and feedback control of vortex shedding using fluidic actuators', Virginia Tech, 2008.
[21] D. M. Luchtenburg, B. R. Noack, M. Schlegel, 'An introduction to the POD Galerkin method for fluid flows with analytical examples and MATLAB source codes', Berlin Inst. Technol., vol. 11, 2009.
[22] C. W. Rowley, T. Colonius, R. M. Murray, 'Model reduction for compressible flows using POD and Galerkin projection', Physica D, vol. 189, no. 1-2, pp. 115–129, 2004. DOI: 10.1016/j.physd.2003.09.040
[23] N. Wiener, 'Extrapolation, Interpolation, and Smoothing of Stationary Time Series: With Engineering Applications', MIT Press, 1949.
[24] C. Hiemstra, J. D. Jones, 'Testing for linear and nonlinear Granger causality in the stock price-volume relation', J. Finance, vol. 49, no. 5, pp. 1639–1664, 1994. DOI: 10.1111/j.1540-6261.1994.tb04776.x
[25] J. R. M. Ding, Y. Chen, S. L. Bressler, 'Granger causality: basic theory and application to neuroscience', in Handbook of Time Series Analysis: Recent Theoretical Developments and Applications, Wiley Online Library, 2006, pp. 437–460.
[26] Freeman, 'Granger causality and the times series analysis of political relationships', Am. J. Polit. Sci., vol. 27, no. 2, pp. 327–358, 1983. DOI: 10.2307/2111025
[27] D. A. Smirnov, I. I. Mokhov, 'From Granger causality to long-term causality: Application to climatic data', Phys. Rev. E, vol. 80, no. 1, pp. 016208, 2009. DOI: 10.1103/PhysRevE.80.016208
[28] J. F. Geweke, 'Measures of conditional linear dependence and feedback between time series', J. Am. Stat. Assoc., vol. 79, no. 388, pp. 907–915, 1984. DOI: 10.1080/01621459.1984.10477105
[29] A. Shojaie, E. B. Fox, 'Granger causality: A review and recent advances', Annu. Rev. Stat. Appl., vol. 9, no. 1, pp. 289–319, 2022. DOI: 10.1146/annurev-statistics-040120-010930
[30] A. Safikhani, A. Shojaie, 'Joint structural break detection and parameter estimation in high-dimensional nonstationary VAR models', J. Am. Stat. Assoc., vol. 117, no. 537, pp. 251–264, 2022. DOI: 10.1080/01621459.2021.2002157
[31] A.Arnold, Y. Liu, N. Abe, 'Temporal causal modeling with graphical granger methods', Proc. 13th ACM SIGKDD Int. Conf. Knowl. Discov. Data Min., pp. 66–75, 2007. DOI: 10.1145/1281192.1281203
[32] A. Shojaie, G. Michailidis, 'Discovering graphical Granger causality using the truncating lasso penalty', Bioinformatics, vol. 26, no. 18, pp. i517–i523, 2010. DOI: 10.1093/bioinformatics/btq377
[33] A. Bolstad, B. D. Van Veen, R. Nowak, 'Causal network inference via group sparse regularization', IEEE Trans. Signal Process., vol. 59, no. 6, pp. 2628–2641, 2011. DOI: 10.1109/TSP.2011.2128315
[34] N. Ancona, D. Marinazzo, S. Stramaglia, 'Radial basis function approach to nonlinear Granger causality of time series', Phys. Rev. E, vol. 70, no. 5, pp. 056221, 2004. DOI: 10.1103/PhysRevE.70.056221
[35] D. Marinazzo, M. Pellicoro, S. Stramaglia, 'Kernel-Granger causality and the analysis of dynamical networks', Phys. Rev. E, vol. 77, no. 5, pp. 056215, 2008. DOI: 10.1103/PhysRevE.77.056215
[36] S. L. Brunton, J. L. Proctor, J. N. Kutz, 'Discovering governing equations from data by sparse identification of nonlinear dynamical systems', Proc. Natl. Acad. Sci., vol. 113, no. 15, pp. 3932–3937, 2016. DOI: 10.1073/pnas.1517384113
[37] H. Akaike, 'Information theory and an extension of the maximum likelihood principle', in Selected Papers of Hirotugu Akaike, Springer, 1998, pp. 199–213.
[38] H. Akaike, 'A Bayesian analysis of the minimum AIC procedure', in Selected Papers of Hirotugu Akaike, Springer, 1998, pp. 275–280.
[39] S. Johansen, 'Statistical analysis of cointegration vectors', J. Econ. Dyn. Control, vol. 12, no. 2-3, pp. 231–254, 1988. DOI: 10.1016/0165-1889(88)90041-3
[40] J. Moehlis, H. Faisst, B. Eckhardt, 'A low-dimensional model for turbulent shear flows', New J. Phys., vol. 6, no. 1, pp. 56, 2004. DOI: 10.1088/1367-2630/6/1/056
[41] T. P. Sapsis, 'Statistics of extreme events in fluid flows and waves', Annu. Rev. Fluid Mech., vol. 53, no. 1, pp. 85–111, 2021. DOI: 10.1146/annurev-fluid-022620-102819
[42] J. D. Skufca, J. A. Yorke, B. Eckhardt, 'Edge of chaos in a parallel shear flow', Phys. Rev. Lett., vol. 96, no. 17, pp. 174101, 2006. DOI: 10.1103/PhysRevLett.96.174101
[43] PA Srinivasan, L Guastoni, H Azizpour, P Schlatter, R Vinuesa, 'Predictions of turbulent shear flows using deep neural networks', Phys. Rev. Fluids, vol. 4, no. 5, pp. 054603, 2019. DOI: 10.1103/PhysRevFluids.4.054603
[44] A. Racca, L. Magri, 'Data-driven prediction and control of extreme events in a chaotic flow', Phys. Rev. Fluids, vol. 7, no. 10, pp. 104402, 2022. DOI: 10.1103/PhysRevFluids.7.104402
[45] R. H. Kraichnan, S. Chen, 'Is there a statistical mechanics of turbulence?', Physica D, vol. 37, no. 1-3, pp. 160–172, 1989. DOI: 10.1016/0167-2789(89)90123-5

[46] M. J. Balajewicz, E. H. Dowell, B. R. Noack, 'Low-dimensional modelling of high-Reynolds-number shear flows incorporating constraints from the Navier–Stokes equation', J. Fluid Mech., vol. 729, pp. 285–308, 2013. DOI: 10.1017/jfm.2013.277
[47] BR Noack, M Schlegel, B Ahlborn, G Mutschke, M Morzyński, P Comte, G Tadmor, 'A finite-time thermodynamics of unsteady fluid flows', Walter de Gruyter GmbH & Co. KG, 2008.
[48] L. Barnett, A. K. Seth, 'The MVGC multivariate Granger causality toolbox: a new approach to Granger-causal inference', J. Neurosci. Methods, vol. 223, pp. 50–68, 2014. DOI: 10.1016/j.jneumeth.2013.10.018